Anomalous Hall Effect and Perpendicular Magnetic Anisotropy in Ultrathin Ferrimagnetic $NiCo_2O_4$ Films

Xuegang Chen,[1,2*] Qiuchen Wu,[1*] Le Zhang,[1] Yifei Hao,[1] Myung-Geun Han,[3] Yimei Zhu,[3] Xia Hong[1,a)]

[1] Department of Physics and Astronomy & Nebraska Center for Materials and Nanoscience, University of Nebraska–Lincoln, Lincoln, NE 68588-0299, USA

[2] Institutes of Physical Science and Information Technology, Anhui University, Hefei 230601, People's Republic of China

[3] Condensed Matter Physics and Materials Science Department, Brookhaven National Laboratory, Upton, NY 11973-5000, USA

[*] These authors contributed equally

[a)] Author to whom correspondence should be addressed: xia.hong@unl.edu

Abstract

The inverse spinel ferrimagnetic $NiCo_2O_4$ possesses high magnetic Curie temperature T_C, high spin polarization, and strain-tunable magnetic anisotropy. Understanding the thickness scaling limit of these intriguing magnetic properties in $NiCo_2O_4$ thin films is critical for their implementation in nanoscale spintronic applications. In this work, we report the unconventional magnetotransport properties of epitaxial (001) $NiCo_2O_4$ films on $MgAl_2O_4$ substrates in the ultrathin limit. Anomalous Hall effect measurements reveal strong perpendicular magnetic anisotropy for films down to 1.5 unit cell (1.2 nm), while T_C for 3 unit cell and thicker films remains above 300 K. The sign change in the anomalous Hall conductivity (σ_{xy}) and its scaling

relation with the longitudinal conductivity (σ_{xx}) can be attributed to the competing effects between impurity scattering and band intrinsic Berry curvature, with the latter vanishing upon the thickness driven metal-insulator transition. Our study reveals the critical role of film thickness in tuning the relative strength of charge correlation, Berry phase effect, spin orbit interaction, and impurity scattering, providing important material information for designing scalable epitaxial magnetic tunnel junctions and sensing devices using $NiCo_2O_4$.

Magnetic thin films with high spin polarization, high Curie temperature, and perpendicular magnetic anisotropy (PMA) are important material solutions for developing high speed energy-efficient spintronics.[1, 2] A promising material candidate is the ferrimagnetic inverse spinel $NiCo_2O_4$ (NCO), where the majority and minority spins are associated with the tetrahedral site Co ions and octahedral site Ni ions, respectively [Fig. 1(a) inset]. Previous studies have shown that epitaxial NCO films exhibit intriguing magnetotransport properties,[3-5] strain tunable magnetic anisotropy,[6] and spin polarization as high as -73%.[7] Being lattice matched with the high performance tunnel barrier candidate, $MgAl_2O_4$, it can be utilized as the spin injection layer for epitaxial magnetic tunnel junctions (MTJ),[7-10] which can potentially suppress the band-folding effect and lead to enhanced tunneling magnetoresistance.[11] Compared with amorphous MTJs, epitaxial NCO/$MgAl_2O_4$/NCO heterostructures also facilitate the understanding of symmetry-based spin filtering effect.[12] Despite the emerging interests in epitaxial NCO thin films,[2-7, 13-18] fundamental understanding of the thickness scaling behavior of its intriguing magnetic properties remains elusive.

In this work, we report the observation of unconventional anomalous Hall effect (AHE) and strong PMA in ultrathin (001) NCO films strained on $MgAl_2O_4$ substrates. The Curie temperature (T_C) of the NCO films remains above 300 K in films as thin as 3 unit cell (uc), while PMA is sustained even in 1.5 uc films. The anomalous Hall (AH) resistance shows a temperature-driven sign change, evolving from clockwise to counterclockwise hysteresis with decreasing temperature. The scaling behavior between the AH conductivity (σ_{xy}) and longitudinal conductivity (σ_{xx}) points to the collective contributions of spin-dependent scattering and band intrinsic Berry phase effect to the AHE in the metallic phase, with the latter vanishing upon the thickness driven metal-insulator transition (MIT).

We deposited epitaxial NCO films on (001) $MgAl_2O_4$ substrates via off-axis radio frequency magnetron sputtering at 320 °C in 100 mTorr processing gas ($Ar:O_2$ = 1:1).[3] X-ray diffraction (XRD) measurements reveal (001)-oriented growth with no impurity phase [Fig. 1(a)]. The Laue oscillations around the Bragg peaks were used to calibrate the growth rate. The *c*-axis lattice constant is 8.20 Å, higher than the bulk value (8.13 Å), which is consistent with a strained film on $MgAl_2O_4$ (a = 8.08 Å).[13, 16] The high crystallinity of the samples is clearly revealed by the high-angle annular dark-field scanning transmission electron microscopy (HAADF-STEM) and selected area electron diffraction (SAED) [Fig. 1(b)]. The as-grown NCO films show smooth surface morphology with a typical surface roughness of 2-3 Å [Fig. 1(c)]. Magnetotransport studies were carried out in van der Pauw device geometry using a Quantum Design Physical Property Measurement System connected with Keithley 2400 SourceMeter or standard lock-in technique (SR830) with low excitation current ($\leqslant$10 μA). We studied two samples for each thickness and the results are highly consistent.

Figure 1(d) shows the temperature dependence of the sheet resistance $R_{\square} = \rho_{xx}/t_{\mathrm{NCO}}$, where ρ_{xx} is the longitudinal resistivity and t_{NCO} is the film thickness, of 1.5-5 uc NCO films. For the 3-5 uc samples, $R_{\square}$ shows a moderate, metallic *T*-dependence ($dR/dT > 0$) below 350 K, consistent with that of thick NCO films.[3, 13, 14] A resistance upturn appears ($dR/dT < 0$) at low temperature, with the upturn temperature (T_{up}) increasing with reducing film thickness. This moderate resistance upturn is the signature behavior of weakly localized conductors, which can be due to electron back-scattering induced quantum interference effect or enhanced electron-electron interaction.[19] The 1.5 uc film becomes insulating over the entire temperature range, with $R_{\square}(T)$ well described by variable range hoping. The transition to the strongly localized behavior occurs in the 2 uc film as $R_{\square}$ approaches $\frac{h}{e^2}$~25.9 kΩ. This thickness-driven MIT has been widely observed in correlated oxide thin films, which may originate from dimensionality crossover,[19, 20] enhanced correlation induced energy gap in ultrathin films,[19, 21] or variation in oxygen octahedral distortion[22] and impurity/defect states[17] at surfaces/interfaces.

Figure 2(a) shows the AHE hysteresis taken in 1.5-5 uc NCO films at 100 K. The Hall resistivity, $\rho_{xy} = R_{xy}t_{\mathrm{NCO}}$ with R_{xy} the Hall resistance, can be decomposed into the normal Hall and AHE contributions: $\rho_{xy} = R_0 H + \rho_{\mathrm{AHE}}$. Here the normal Hall coefficient $R_0 = 1/en_{\mathrm{eff}}$ yields the effective carrier density n_{eff}, *H* is the out-of-plane magnetic field, and ρ_{AHE} is the AH resistivity. All samples exhibit counterclockwise AHE hysteresis, which is defined as positive. The coercive field (H_c) is significantly reduced in the 1.5 and 2 uc films [Fig. 2(b)], which may be attributed to domain nucleation and domain wall motion promoted by interfacial defects[23] and/or enhanced thermal fluctuation with reduced dimension. The sharp switching of the AHE hysteresis suggests that PMA is preserved in NCO films as thin as 1.5 uc. This can be well accounted for by the 0.6% compressive strain for (001) NCO on $MgAl_2O_4$, which yields ~1 meV magnetic

anisotropic energy between the in-plane and out-of-plane orientations, well exceeding the shape anisotropy (~μeV).[3, 6, 14] From the temperature dependence of ρ_{AHE}, we found that T_C is above 300 K for the 3-5 uc NCO films and decreases to 230 K for the 2 uc (1.6 nm) NCO and 170 K for the 1.5 uc (1.2 nm) film [Fig. 2(c)]. Figure 2(d) compares the T_C at the ultrathin limit for epitaxial thin films of magnetic complex oxides, such as $SrRuO_3$ (SRO)[24] and $La_{0.7}Sr_{0.3}MnO_3$ (LSMO),[25] and two-dimensional (2D) van der Waals (vdW) magnets, including VSe_2,[26] $MnSe_2$,[27] $CrSe_2$,[28] CrI_3,[29] $CrCl_3$,[30] Fe_3GeTe_2 (FGT),[31, 32] and $Cr_2Ge_2Te_6$ (CGT).[33] Both classes of material systems are well suited to build crystalline heterostructures based on structurally similar yet functionally distinct constituents.[34, 35] The combined high T_C and strong PMA of ultrathin NCO films outperform most magnetic complex oxides. Compared to 2D vdW magnets, it offers not only highly competitive material parameters but also the distinct advantage of scalable growth, where high quality epitaxial ultrathin films can be controlled with atomic precision.[36] These features make NCO a highly promising material candidate for developing nanoscale multifunctional applications.

One intriguing property of NCO is the AHE exhibits a nonmonotonic T-dependence that leads to temperature/film thickness driven sign change in ρ_{AHE}.[3] Figure 3(a) shows R_{xy} of a 2 uc film at various temperatures. Below T_C of 230 K, R_{xy} exhibits a non-linear H-dependence, signaling the appearance of AHE. The magnitude of AH resistance $R_{\mathrm{AHE}} = \rho_{\mathrm{AHE}}/t_{\mathrm{NCO}}$ first increases below T_C, which can be attributed to the initial rapid growth of magnetization. After reaching a local maximum at 190 K, R_{AHE} starts to decrease with decreasing temperature, and crosses zero at T_{sc} = 150 K. Similar T-dependence of R_{AHE} has been observed in all ultrathin films [Fig. 3(b)]. The transition from the negative (clockwise) to positive (counterclockwise) hysteresis occurs smoothly without any abrupt jump in R_{AHE} [Fig. 3(c)], and the sign change temperature T_{sc} does not exhibit an apparent dependence on film thickness [Fig. 2(c)]. As NCO is a multiband conductor,[15] we also

examined n_{eff} from the high field (up to 50 kOe) normal Hall effect. Figure 3(d) reveals a transition from electron-like ($R_0 < 0$) to hole-like ($R_0 > 0$) behavior upon cooling for the 2 uc sample. The transition temperature is about 200 K, much higher than T_{sc}, ruling out the change of carrier type as the origin of R_{AHE} sign change. We also extracted H_c from the AHE hysteresis. The exponential T-dependence [Fig. 3(e)] points to thermally activated domain wall depinning.[23] The smooth T-dependences of R_{AHE} and H_c [Fig. 3(f)] indicate that the sign change in AHE is not induced by an abrupt change of magnetic state in the samples.

Previous studies of thick NCO films show that the sign change phenomenon can result from the competition between multiple AHE mechanisms.[3] Based on quantum transport theory of multiband magnetic conductors, the scaling relation between σ_{xy} and σ_{xx} depends on the relative strength of impurity scattering rate with respect to the Fermi energy:[37]

$$\sigma_{xy} = \text{constant} ; \quad (1a)$$

$$\sigma_{xy} \propto \sigma_{xx}^{1.6}. \quad (1b)$$

Equation (1a) describes the scattering-independent band intrinsic Berry phase contribution to AHE, which dominates in moderately dirty metals.[37] Equation (1b) depicts the impurity scattering dominated behavior in dirty metals.[37, 38] For thick NCO films, σ_{xx} is close to the boundary between these two regions ($\sigma_{xx}\sim 10^3\ \Omega^{-1}\mathrm{cm}^{-1}$), and both mechanisms can coexist. For super-clean metals ($\sigma_{xx} \gtrsim 10^6\ \Omega^{-1}\mathrm{cm}^{-1}$), the skew scattering mechanism arises due to the spin-orbit interaction associated with impurities, which yields a linear dependence between σ_{xx} and σ_{xy}can also give rise to a linear dependence between σ_{xx} and σ_{xy}.[37] This mechanism is less likely to be prominent in NCO, which is prone to formation of various disorders due to its multi-cation, multivalence nature.[2, 4, 15-18]

Figure 4(a) shows σ_{xy} *vs.* σ_{xx} for the ultrathin NCO films, where σ_{xx} is extracted from the zero-field $R_{\square}(T)$ [Fig. 1(d)] and $\sigma_{xy} = \rho_{\mathrm{AHE}}/\rho_{xx}^2$. A clear power-law dependence is present in all samples in the intermediate temperature range with the exponent close to 1.6. We fitted the scaling relation by considering both the impurity scattering and band intrinsic contributions:

$$\sigma_{xy} = A_1\sigma_{xx}^{1.6} + \sigma_{xy}^{(0)}. \quad (2)$$

Here A_1 is the fitting parameter and $\sigma_{xy}^{(0)}$ is the Berry phase contribution.[37-40] The band intrinsic nature of the latter has been confirmed in thick films from the scaling behavior between σ_{xy} and magnetization.[5] For the 3-5 uc films in the metallic region above T_{up}, the power law scaling between σ_{xy} and σ_{xx} can be well depicted by Eq. (2). The sign of σ_{xy} is thus determined by the relative strength of the positive contribution from dirty metal scattering and the negative Berry phase contribution. With reducing film thickness, σ_{xx} decreases, moving further away from the boundary to the moderately dirty region. This is consistent with the rising contribution from impurity scattering (A_1), while the intrinsic contribution $\sigma_{xy}^{(0)}$ only shows a slight increase [Fig. 4(b)]. Below T_{up}, σ_{xy} exhibits very weak T-dependence. In addition to the band intrinsic effect, spin-orbit interaction in impurity scattering, known as the side jump effect $\sigma_{xy}^{(1)}$, may also lead to the scattering insensitive AHE in this region. Overall, the AHE for films of this thickness range (3-5 uc) is qualitatively similar to that observed in thicker films.[3]

The 1.5-2 uc NCO films, on the other hand, exhibit distinct σ_{xy} *vs.* σ_{xx} scaling relation. The 2 uc film exhibits a MIT as $R_{\square}$ exceeds $\frac{h}{e^2}$. While the high temperature AHE scaling still follows Eq. (2), there is a sharp increase in A_1. Below T_{up}, σ_{xx} falls rapidly and the AHE can be well described by the dirty metal scaling relation alone:

$$\sigma_{xy} = A_2\sigma_{xx}^{1.6}. \quad (3)$$

Similar scaling is observed in the insulating, 1.5 uc sample, where the negligible contribution of the Berry phase term is corroborated by the facts that T_{sc} approaches T_C [Fig. 2(c)] and the sign change behavior is hard to resolve [Fig. 3(c)]. Equation (3) is qualitatively different from the σ_{xx}-independent σ_{xy} observed in the weakly localized regime of thicker films below T_{up}, and can be well accounted for by phonon-assisted hopping and percolative transport.[19, 41, 42] It further shows that the spin scattering source is likely associated with the surface/interface of the sample, whose contribution becomes dominant in ultrathin films.

Based on this scenario, we summarized the AHE mechanisms observed in the ultrathin NCO films as well as previously studied thick films.[3] Figure 4(c) shows the temperature-film thickness diagram for the electronic and magnetic state of 1.5-30 uc NCO films. For 2 uc and thicker films, the intermediate temperature region between T_C and T_{up} corresponds to a metallic phase, and the AHE depends on the collective contributions of band intrinsic effect and impurity scattering. Below T_{up}, R_{AHE} becomes independent of scattering, which can be due to the Berry phase and/or side jump effect. Upon the onset of strong localization ($R_{\square} > \frac{h}{e^2}$),[19, 43] the Berry phase effect vanishes, and the dirty metal scaling behavior dominates R_{AHE}. The rich electronic/AHE diagram is thus a clear manifestation of the complex energy landscape in NCO associated with magnetic exchange, electron correlation, spin-orbit interaction, and impurity scattering. The film thickness offers an effective control parameter to tune the relative strength between these energy scales, which can be utilized to design application-specific magnetic properties, including the magnetic transition temperature, coercive field, and the strength and sign of AH effect.

In summary, we show that epitaxial NCO films as thin as 1.5 uc (1.2 nm) can sustain strong PMA, competitive T_C of 170 K, and robust AH effect. The AHE reveals the complex interplay between band intrinsic Berry phase effect and impurity scattering, while the film thickness can be leveraged to tune their relative strength. Our study also paves the path for scalable development of NCO based epitaxial MTJs and sensor devices.

Acknowledgements

This work was primarily supported by National Science Foundation through Grant No. DMR-1710461 and EPSCoR RII Track-1: Emergent Quantum Materials and Technologies (EQUATE), Award OIA-2044049. Work by X. Chen was partially supported by the National Natural Science Foundation of China (Grants No. 12104005). Work by M.H. and Y.Z. was supported by the Materials Science and Engineering Divisions, Office of Basic Energy Sciences of the U.S. Department of Energy under Contract No. DESC0012704. TEM sample preparation using FIB was performed at the Center for Functional Nanomaterials, Brookhaven National Laboratory. The research was performed in part in the Nebraska Nanoscale Facility: National Nanotechnology Coordinated Infrastructure and the Nebraska Center for Materials and Nanoscience, which are supported by the National Science Foundation under Award ECCS: 2025298, and the Nebraska Research Initiative.

Conflict of Interest

The authors have no conflicts to disclose.

Reference:

[1] T. Dietl, A ten-year perspective on dilute magnetic semiconductors and oxides, Nature Materials **9**, 965 (2010).

[2] P. Li, C. Xia, J. Li, Z. Zhu, Y. Wen, Q. Zhang, J. Zhang, Y. Peng, H. N. Alshareef, and X. Zhang, Spin Filtering in Epitaxial Spinel Films with Nanoscale Phase Separation, ACS nano **11**, 5011 (2017).

[3] X. Chen, X. Zhang, M.-G. Han, L. Zhang, Y. Zhu, X. Xu, and X. Hong, Magnetotransport Anomaly in Room-Temperature Ferrimagnetic $NiCo_2O_4$ Thin Films, Advanced Materials **31**, 1805260 (2019).

[4] M. Xue, X. Chen, S. Ding, Z. Liang, Y. Peng, X. Li, L. Zha, W. Yang, J. Han, S. Liu, et al., Transport Anomaly in Perpendicular Magnetic Anisotropic $NiCo_2O_4$ Thin Films with Column-like Phase Separation, ACS Applied Electronic Materials **2**, 3964 (2020).

[5] D. Kan, L. Xie, and Y. Shimakawa, Scaling of the anomalous Hall effect in perpendicularly magnetized epitaxial films of the ferrimagnet $NiCo_2O_4$, Physical Review B **104**, 134407 (2021).

[6] C. Mellinger, J. Waybright, X. Zhang, C. Schmidt, and X. Xu, Perpendicular magnetic anisotropy in conducting $NiCo_2O_4$ films from spin-lattice coupling, Physical Review B **101**, 014413 (2020).

[7] Y. Shen, D. Kan, I.-C. Lin, M.-W. Chu, I. Suzuki, and Y. Shimakawa, Perpendicular magnetic tunnel junctions based on half-metallic $NiCo_2O_4$, Applied Physics Letters **117**, 042408 (2020).

[8] B. Dieny and M. Chshiev, Perpendicular magnetic anisotropy at transition metal/oxide interfaces and applications, Reviews of Modern Physics **89**, 025008 (2017).

[9] J. Zhang, X. G. Zhang, and X. F. Han, Spinel oxides: Δ 1 spin-filter barrier for a class of magnetic tunnel junctions, Applied Physics Letters **100**, 222401 (2012).

[10] H. Sukegawa, Y. Miura, S. Muramoto, S. Mitani, T. Niizeki, T. Ohkubo, K. Abe, M. Shirai, K. Inomata, and K. Hono, Enhanced tunnel magnetoresistance in a spinel oxide barrier with cation-site disorder, Physical Review B **86**, 184401 (2012).

[11] Y. Miura, S. Muramoto, K. Abe, and M. Shirai, First-principles study of tunneling magnetoresistance in $Fe/MgAl_2O_4/Fe(001)$ magnetic tunnel junctions, Physical Review B **86**, 024426 (2012).

[12] M. Bibes, J. E. Villegas, and A. Barthelemy, Ultrathin oxide films and interfaces for electronics and spintronics, Adv. Phys. **60**, 5 (2011).

[13] P. Silwal, L. Miao, I. Stern, X. Zhou, J. Hu, and D. Ho Kim, Metal insulator transition with ferrimagnetic order in epitaxial thin films of spinel $NiCo_2O_4$, Applied Physics Letters **100**, 032102 (2012).

[14] P. Silwal, L. Miao, J. Hu, L. Spinu, D. Ho Kim, and D. Talbayev, Thickness dependent structural, magnetic, and electronic properties of the epitaxial films of transparent conducting oxide $NiCo_2O_4$, Journal of Applied Physics **114**, 103704 (2013).

[15] K. Dileep, B. Loukya, P. Silwal, A. Gupta, and R. Datta, Probing optical band gaps at nanoscale from tetrahedral cation vacancy defects and variation of cation ordering in $NiCo_2O_4$ epitaxial thin films, Journal of Physics D: Applied Physics **47**, 405001 (2014).

[16] Y. Bitla, Y. Y. Chin, J. C. Lin, C. N. Van, R. Liu, Y. Zhu, H. J. Liu, Q. Zhan, H. J. Lin, C. T. Chen, et al., Origin of metallic behavior in $NiCo_2O_4$ ferrimagnet, Scientific reports **5**, 15201 (2015).

[17] C. M. Zhen, X. Z. Zhang, W. G. Wei, W. Z. Guo, A. Pant, X. S. Xu, J. Shen, L. Ma, and D. L. Hou, Nanostructural origin of semiconductivity and large magnetoresistance in epitaxial $NiCo_2O_4/Al_2O_3$ thin films, Journal of Physics D-Applied Physics **51**, 145308 (2018).

[18] Y. Shen, D. Kan, Z. Tan, Y. Wakabayashi, and Y. Shimakawa, Tuning of ferrimagnetism and perpendicular magnetic anisotropy in $NiCo_2O_4$ epitaxial films by the cation distribution, Physical Review B **101**, 094412 (2020).

[19] L. Zhang, X. Jiang, X. Xu, and X. Hong, Abrupt enhancement of spin–orbit scattering time in ultrathin semimetallic SrIrO3 close to the metal–insulator transition, APL Materials **8**, 051108 (2020).

[20] R. Scherwitzl, S. Gariglio, M. Gabay, P. Zubko, M. Gibert, and J. M. Triscone, Metal-Insulator Transition in Ultrathin $LaNiO_3$ Films, Physical Review Letters **106**, 246403 (2011).

[21] D. Groenendijk, C. Autieri, J. Girovsky, M. C. Martinez-Velarte, N. Manca, G. Mattoni, A. Monteiro, N. Gauquelin, J. Verbeeck, and A. J. P. r. l. Otte, Spin-orbit semimetal $SrIrO_3$ in the two-dimensional limit, Physical Review Letters **119**, 256403 (2017).

[22] A. Rajapitamahuni, L. Zhang, M. A. Koten, V. Singh, J. D. Burton, E. Y. Tsymbal, J. E. Shield, and X. J. P. r. l. Hong, Giant enhancement of magnetic anisotropy in ultrathin manganite films via nanoscale 1D periodic depth modulation, Physical Review Letters **116**, 187201 (2016).

[23] P. J. Metaxas, J. P. Jamet, A. Mougin, M. Cormier, J. Ferre, V. Baltz, B. Rodmacq, B. Dieny, and R. L. Stamps, Creep and flow regimes of magnetic domain-wall motion in ultrathin Pt/Co/Pt films with perpendicular anisotropy, Phys. Rev. Lett. **99**, 217208 (2007).

[24] J. Xia, W. Siemons, G. Koster, M. R. Beasley, and A. Kapitulnik, Critical thickness for itinerant ferromagnetism in ultrathin films of $SrRuO_3$, Physical Review B **79**, 140407 (2009).

[25] M. Huijben, L. W. Martin, Y. H. Chu, M. B. Holcomb, P. Yu, G. Rijnders, D. H. A. Blank, and R. Ramesh, Critical thickness and orbital ordering in ultrathin $La_{0.7}Sr_{0.3}MnO_3$ films, Physical Review B **78**, 094413 (2008).

[26] M. Bonilla, S. Kolekar, Y. Ma, H. C. Diaz, V. Kalappattil, R. Das, T. Eggers, H. R. Gutierrez, M.-H. Phan, and M. Batzill, Strong room-temperature ferromagnetism in VSe_2 monolayers on van der Waals substrates, Nature Nanotechnology **13**, 289 (2018).

[27] D. J. O'Hara, T. Zhu, A. H. Trout, A. S. Ahmed, Y. K. Luo, C. H. Lee, M. R. Brenner, S. Rajan, J. A. Gupta, D. W. McComb, et al., Room Temperature Intrinsic Ferromagnetism in Epitaxial Manganese Selenide Films in the Monolayer Limit, Nano Letters **18**, 3125 (2018).

[28] B. Li, Z. Wan, C. Wang, P. Chen, B. Huang, X. Cheng, Q. Qian, J. Li, Z. Zhang, G. Sun, et al., Van der Waals epitaxial growth of air-stable $CrSe_2$ nanosheets with thickness-tunable magnetic order, Nature Materials **20**, 818 (2021).

[29] B. Huang, G. Clark, E. Navarro-Moratalla, D. R. Klein, R. Cheng, K. L. Seyler, D. Zhong, E. Schmidgall, M. A. McGuire, D. H. Cobden, et al., Layer-dependent ferromagnetism in a van der Waals crystal down to the monolayer limit, Nature **546**, 270 (2017).

[30] X. Cai, T. Song, N. P. Wilson, G. Clark, M. He, X. Zhang, T. Taniguchi, K. Watanabe, W. Yao, D. Xiao, et al., Atomically Thin $CrCl_3$: An In-Plane Layered Antiferromagnetic Insulator, Nano Letters **19**, 3993 (2019).

[31] Z. Fei, B. Huang, P. Malinowski, W. Wang, T. Song, J. Sanchez, W. Yao, D. Xiao, X. Zhu, A. F. May, et al., Two-dimensional itinerant ferromagnetism in atomically thin Fe_3GeTe_2, Nature Materials **17**, 778 (2018).

[32] Y. Deng, Y. Yu, Y. Song, J. Zhang, N. Z. Wang, Z. Sun, Y. Yi, Y. Z. Wu, S. Wu, J. Zhu, et al., Gate-tunable room-temperature ferromagnetism in two-dimensional Fe_3GeTe_2, Nature **563**, 94 (2018).

[33] C. Gong, L. Li, Z. Li, H. Ji, A. Stern, Y. Xia, T. Cao, W. Bao, C. Wang, Y. Wang, et al., Discovery of intrinsic ferromagnetism in two-dimensional van der Waals crystals, Nature **546**, 265 (2017).

[34] A. K. Geim and I. V. Grigorieva, Van der Waals heterostructures, Nature **499**, 419 (2013).

[35] H. Y. Hwang, Y. Iwasa, M. Kawasaki, B. Keimer, N. Nagaosa, and Y. Tokura, Emergent phenomena at oxide interfaces, Nature Materials **11**, 103 (2012).

[36] X. G. Chen, X. Zhang, M. A. Koten, H. H. Chen, Z. Y. Xiao, L. Zhang, J. E. Shield, P. A. Dowben, and X. Hong, Interfacial Charge Engineering in Ferroelectric-Controlled Mott Transistors, Advanced Materials **29**, 1701385 (2017).

[37] S. Onoda, N. Sugimoto, and N. Nagaosa, Quantum transport theory of anomalous electric, thermoelectric, and thermal Hall effects in ferromagnets, Physical Review B **77**, 165103 (2008).

[38] T. Fukumura, H. Toyosaki, K. Ueno, M. Nakano, T. Yamasaki, and M. Kawasaki, A scaling relation of anomalous Hall effect in ferromagnetic semiconductors and metals, Japanese Journal of Applied Physics **46**, L642 (2007).

[39] A. A. Kovalev, J. Sinova, and Y. Tserkovnyak, Anomalous Hall effect in disordered multiband metals, Physical Review Letters **105**, 036601 (2010).

[40] S. Onoda, N. Sugimoto, and N. Nagaosa, Intrinsic versus extrinsic anomalous Hall effect in ferromagnets, Physical Review Letters **97**, 126602 (2006).

[41] A. A. Burkov and L. Balents, Anomalous Hall effect in ferromagnetic semiconductors in the hopping transport regime, Phys. Rev. Lett. **91**, 057202 (2003).

[42] X.-J. Liu, X. Liu, and J. Sinova, Scaling of the anomalous Hall effect in the insulating regime, Physical Review B **84** (2011).

[43] X. Hong, S. H. Cheng, C. Herding, and J. Zhu, Colossal negative magnetoresistance in dilute fluorinated graphene, Physical Review B **83**, 085410 (2011).

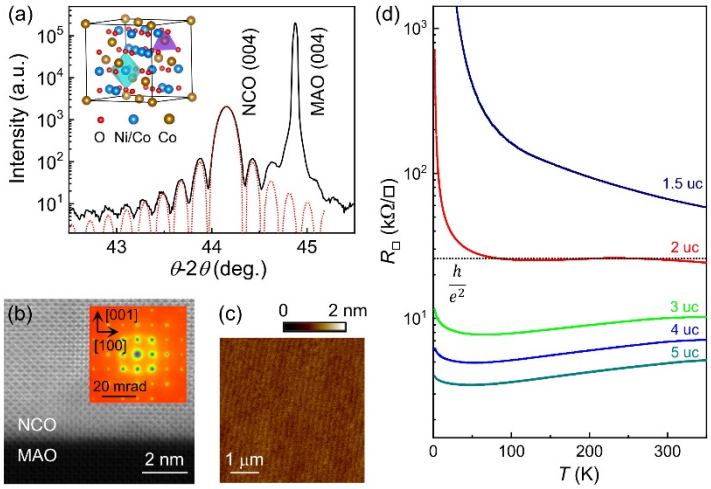

FIG. 1. (a) XRD θ-2θ scan of a 60 uc NCO film on MAO with a fit to Laue oscillations near the (004) peak (dotted line). Inset: Schematic of NCO crystal structure. (b) HAADF-STEM and (inset) SAED images taken on a 17 uc NCO. (c) AFM topography image of a 5 uc NCO showing atomically flat terraces. (d) $R_{\square}(T)$ for 1.5-5 uc films. The dotted line illustrates the two-dimensional quantum resistance $\frac{h}{e^2}$.

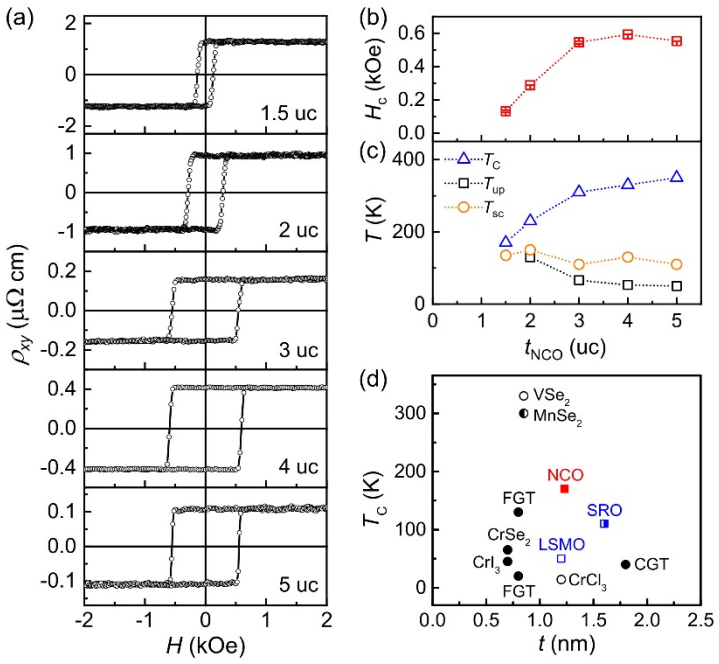

FIG. 2. (a) ρ_{xy} *vs* H hysteresis at 100 K for 1.5-5 uc NCO. (b-c) t_{NCO}-dependence of (b) H_C at 100 K, and (c) T_C, T_{up}, and T_{sc}. (d) T_C *vs.* thickness for epitaxial complex oxide films (squares)[24,25] and 2D vdW magnets (circles).[26-33] Solid symbols: PMA. Open symbols: in-plane MA.

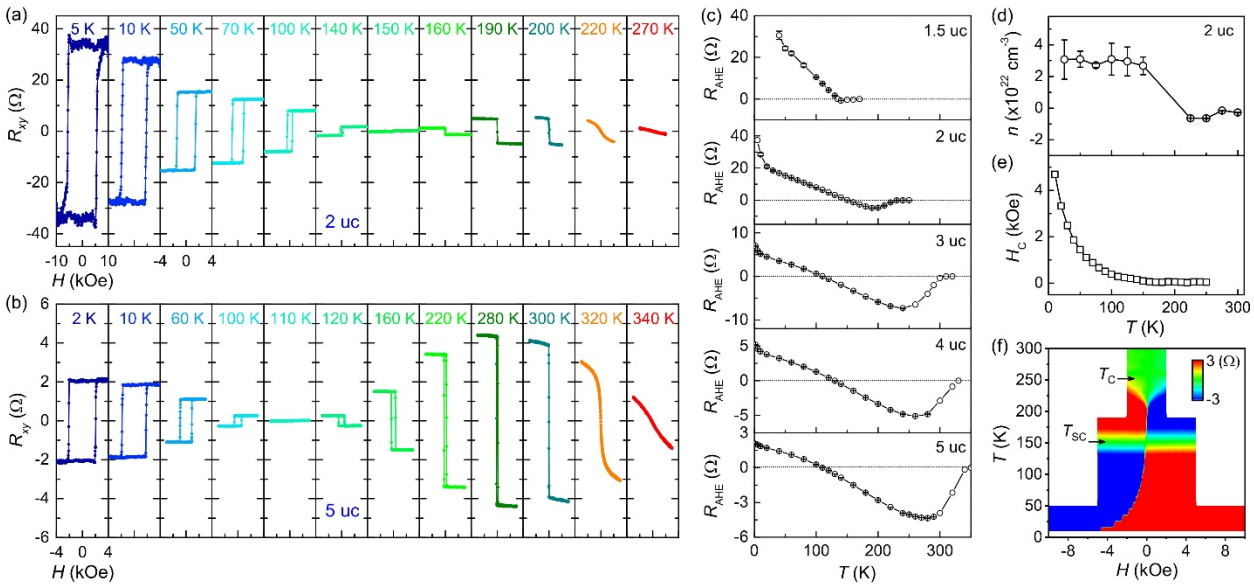

FIG. 3. (a) AHE of 2 uc NCO at various temperatures. Field range: ±10 kOe for 5-10 K and ±4 kOe for higher temperatures. (b) AHE of 5 uc NCO at various temperatures. (c) R_{AHE} *vs. T* for 1.5-5 uc NCO. (d) *n vs. T* and (e) H_c *vs. T* for 2 uc NCO. (f) R_{xy} *vs. T* and *H* (sweeping down) for 2 uc NCO.

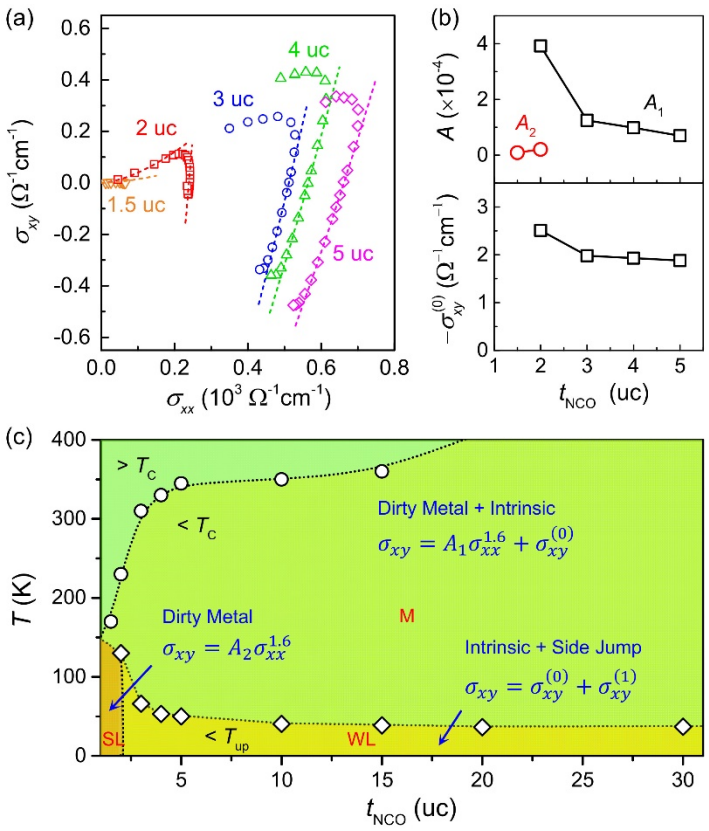

FIG 4. (a) σ_{xy} *vs.* σ_{xx} for 1.5-5 uc NCO films with fits to Eqs. (2)-(3) (dash lines). (b) t_{NCO}-dependence of A_1, A_2 and $\sigma_{xy}^{(0)}$. (c) Temperature-thickness diagram of the AHE scaling behavior. M: metallic. WL: weakly localized. SL: strongly localized. The data for 10-30 uc films are taken from Ref. [3].